# Widespread volcanism in the Greenland-North Atlantic region explained by the Iceland plume

Bernhard Steinberger[1,2,*], Eva Bredow[1,3], Sergei Lebedev[4], Andrew Schaeffer[5] & Trond H. Torsvik[2,1,6,7]

[1]*Section 2.5 Geodynamic Modelling, GFZ German Research Centre for Geosciences, Potsdam, Germany.*

[2]*Centre for Earth Evolution and Dynamics (CEED), University of Oslo, Oslo, Norway.*

[3]*Current Address: Institute of Geosciences, Christian-Albrechts-Universitt Kiel, Germany.*

[4]*Dublin Institute for Advanced Studies, School of Cosmic Physics, Geophysics Section, Dublin, Ireland.*

[5]*Department of Earth Science, University of Ottawa, Ottawa, Canada.*

[6]*Geological Survey of Norway (NGU), Trondheim, Norway*

[7]*School of Geosciences, University of Witwatersrand, Wits, South Africa*

**In the classical concept, a hotspot track is a line of volcanics, formed as a plate moves over a stationary mantle plume. Defying this concept, intraplate volcanism in Greenland and the North Atlantic region occurred simultaneously over a wide area, particularly around 60 million years ago, and showing no resemblance to a hotspot track. Here we show that most of this volcanism can, nonetheless, be explained solely by the Iceland plume, interacting with sea floor spreading ridges, global mantle flow and a lithosphere – the outermost rigid layer of the Earth – with strongly variable thickness. An east-west corridor of thinned lithosphere across central Greenland, as inferred from new, highly resolved tomographic images, could have**

**formed as Greenland moved westward over the Iceland plume between 90 and 60 million years ago. Our numerical geodynamic model demonstrates how plume material may have accumulated in this corridor and in areas east and west of Greenland. Simultaneous plume-related volcanic activities starting about 62 million years ago on either side of Greenland could occur where and when the lithosphere was thin enough due to continental rifting and sea floor spreading, possibly long after the plume reached the base of the lithosphere.**

Around 62 million year ago (Ma), simultaneous volcanism started in Western Greenland[1], Baffin Island[2], Eastern Greenland and the British Isles[3] (Fig. 1, inset histogram). High $^{3}He/^{4}He$ ratios in all these regions[2,4–6] are indicative of a mantle plume origin or contribution. The age distribution of volcanics peaks around 55 Ma, and it remains an open question whether this voluminous and widespread volcanism was caused by a single plume – either the plume head[7] or a preexisting plume[8,9] – and, if so, where it was positioned, and how large it was. When reconstructing plates to their location at 60 Ma (Fig. 2), it becomes evident that plume material would still need to flow for more than 1000 km from a putative plume centre beneath Eastern Greenland to some of the locations where volcanism occurred. Alternatives to this single-plume hypothesis could be that there are more than one plume responsible such as Jan Mayen[10], Canary or Azores[11], a more sheetlike upwelling extended in north-south direction[12], or that excess volcanism is caused by processes other than a mantle plume[13,14]. The subject has been extensively reviewed[15,16].

Presently, Iceland is an anomaly along the Mid-Atlantic Ridge, with much thicker crust than normal sea floor, caused by the more intensive volcanism. Seismic tomography models show

evidence for a hot upwelling in the upper mantle[20]; some tomography models also indicate a lower mantle origin[21,22], with the position of Iceland near the northern tip of the African Large Low Shear Velocity Province (LLSVP) a likely location from which the plume rises[23].

To address the question how much of the widespread volcanism around 60 Ma can be explained by the Iceland plume as single source, we combine recent results from plate reconstructions, seismic tomography and geodynamic modelling to assess where the plume impacted and how and where plume material could have flowed beneath the lithosphere so as to give rise to the observed volcanism. The sub-lithospheric flow of hot asthenosphere is strongly influenced by the location of the plume relative to spreading ridges[24] and by variations in lithosphere thickness[25], which can be estimated for the past by combining seismic tomography with plate reconstructions. We will discuss how combining these ingredients may help qualitatively explain the distribution of volcanics. The discussion will be supplemented by numerical simulations.

## Conceptual model of plume-lithosphere interaction

The motion of the Iceland plume is controlled by large-scale flow, which tilts and distorts the plume conduit as it rises through the slowly convecting mantle. When this motion is taken into account, models typically predict that around 60 Myr ago the Iceland plume was a few hundred km further east in the mantle than its present location, and has moved westward according to the predominant flow direction at the top of the lower mantle[17,26]. At shallower depth beneath the lithosphere, an overall large-scale flow in a north-northwestern direction is consistent with the location of Iceland

relative to the LLSVP, tomographic images[23] and shear wave splitting results[27,28].

When the plate and plume motions are added, it turns out that the Iceland plume was most likely located beneath eastern[17,29] (Fig. 2) or central[30] Greenland around 60 Ma. For comparison, assuming a fixed plume has led to a predicted location in western Greenland[31], although even earlier models[32,33] also predicted a plume location in eastern Greenland at that time.

Present-day lithosphere thickness can be inferred from seismic tomography or sea floor ages. Using models of plate motion, past lithosphere thickness can be reconstructed (see Methods). The left panel of Fig. 2 shows a 60 Ma reconstruction. Present-day thickness based on tomography only is shown in the right panel, and Fig. S1 shows reconstructions for other times.

The qualitative scenario that emerges if we combine models of plume motion, lithosphere thickness through time and large-scale mantle flow is similar to Vink's[32] in that the Iceland plume has been close to the North Atlantic spreading ridge since the initiation of spreading, and therefore the most voluminous volcanism did not occur directly above the plume but at the ridge location closest to the plume. This first formed the Vøring Plateau offshore Central Norway (Fig. 1) and later on the Greenland-Faeroe plateau. In contrast, the Ægir ridge in between was never closest to the plume (see Fig. S1), hence it has close to normal crustal thickness.

Critically, where plume material is flowing to and where it comes close to the surface, and hence where volcanism can be expected, is affected by large-scale flow and lithosphere thickness. An east-west oriented thin-lithosphere corridor that we see in our models provides a simple yet

elegant mechanism for how a single plume could feed roughly simultaneous volcanism on the east and west coasts of Greenland. This corridor is evident when looking at the tomography model AMISvArc which shows significantly reduced seismic velocities where the passage of the Iceland plume has been inferred, indicative of relatively warmer and thinner lithosphere[34] (Fig. 3). Hot asthenosphere could flow westward following this corridor and, furthermore, the corridor itself could have been created by the earlier Late Cretaceous passage of Greenland over the plume (Fig. 2 right), thus accumulating and trapping plume material in this corridor underneath thick continental lithosphere. Even earlier, the plume track follows the West coast of Greenland, where subsequently Baffin Bay opened, and around 130-120 Ma, parts of the High Arctic Large Igneous Province, Ellesmere and Svalbard[19] are reconstructed near the plume location, as is evident from the plume track in Fig. 2, and could therefore be causally linked to the Iceland plume (see also [9]).

Although the lithosphere thickness may have changed during the rifting process, our reconstruction indicates that there may have already been a region of thin lithosphere between Greenland and Europe – even though they were much closer to each other – especially south of the plume, at 60 Ma. Material from the plume could then have been channelled along that corridor and led to volcanism in the British Tertiary Igneous Province[38] at $\approx$ 60 Ma.

**Plume melting below a moving lithosphere of variable thickness**

In order to assess the spatial distribution and amount of basaltic volcanism due to a plume interacting with moving lithospheric plates of variable thickness and nearby spreading ridges, we set

up a regional numerical model, using recently developed and validated methods[39,40]. The plume is initiated with a large plume head at the base of the upper mantle at either 64 Ma (Model64Ma) or 115 Ma (Model115Ma). In Model64Ma we adopt the plume and plate motions from ref.[29], corresponding to the hotspot track in Fig. 5 right, whereas in Model115 the plume location has been modified, and displaced 300 km westward 70-60 Ma to obtain a smoother track. A global mantle flow model derived from tomography converted to density anomalies is used as boundary condition for our regional model. The model is initiated with a reconstructed lithosphere thickness distribution. More details are described in the methods section.

Fig. 4 shows results for 68 Ma and 59 Ma for Model115Ma. At 68 Ma, plate motions are divergent between Greenland and North America. The plume has spread widely beneath the lithosphere, and trapped large amounts of hot material in the corridor across Greenland, above which the continental lithosphere is relatively thin, but too thick to enable melting. An arm extends to the south along the rift between Greenland and North America plates. At 59 Ma, accelerated rifting has started beneath Greenland and Europe, and volcanic activity occurs simultaneously both east and west of Greenland, as soon as the ponded plume material reaches areas where thin lithosphere and decompression along the mid-ocean ridges enable melting. This marks the onset of intense plume-ridge interaction, which is supported by plate motions and mantle flow, and continues until the present-day state of the model. The resulting total amount of plume-related melt in Model115Ma is shown in Fig. 5 (left) and compared with a crustal thickness map derived from gravity inversion (Fig. 5 right[17]). Features that are common to both maps include relatively thick crust along the Iceland-Greenland Ridge, the Iceland-Faroe Ridge, the Norwegian continental margin, and on the

Jan Mayen Microcontinent. The thickest oceanic crust occurs in the southeastern part of Iceland in both maps.

The distribution of melt produced in different time intervals is shown in Fig. 6 and compared to locations of dated volcanics of same age. For Model64Ma (Fig. 6 top left), where the plume has always been beneath Eastern Greenland or the Atlantic, volcanism only occurs within or near the opening Atlantic. However, for Model115Ma, simultaneous volcanism around 60-45 Ma also occurs in Baffin Bay west of Greenland (Figs. 6 and 5). Despite the much earlier impingement of the plume beneath the lithosphere, the first plume-related volcanics in this model only occur at 80 Ma in the Labrador Sea, and after $\approx$ 60 Ma, somewhat later than observed, in the North Atlantic and Baffin Bay. Before that, plume material spreads beneath thick lithosphere, without any melt generation. Only after 60 Ma, due to rifting and incipient spreading, the lithosphere in Baffin Bay has sufficiently thinned such that the first melts are produced. At the same time, Greenland has moved westward, such that the plume is located sufficiently close to the nascent North Atlantic and can also produce melts there. Melting in Baffin Bay continues until the time interval 55-45 Ma in Model115Ma. For melting to occur west of Greenland, it is not necessary to assume a plume initiation as early as 115 Ma. For example, if Iceland plume initiation occurs at 64 Ma beneath central Greenland, 600 km west of Model64Ma the plume head also spreads across Greenland and leads to volcanism on both sides (results not shown).

## Lateral flow and long delays from plume impact to volcanism

Interaction of a plume head or large pulse with a lithosphere of strongly variable thickness can create a distribution of volcanics very different from a classical hotspot track. If the Iceland plume was located near the Eastern continental margin of Greenland around 60 Ma, a pulse at that time would have caused volcanism mainly along the opening rift between Greenland and Europe. Our numerical model yields plume-induced volcanics along a large stretch of the rift that developed into the North Atlantic – on the European side until the western margin of the Rockall Plateau, more than 1000 km towards the southwest of the plume. This is not necessarily all plume material; the plume also pushes material ahead and hence changes the flow field elsewhere. This may lead to melting where the asthenosphere flows from beneath thick to thin lithosphere. Assuming today's lithospheric thickness in Greenland, a plume head that impinged near the East Greenland margin around 60 Ma does not lead to volcanism west of Greenland around that time. However, if the plume has pre-existed, a sufficient amount of hot plume material may have accumulated, particularly along a corridor of relatively thin lithosphere inferred from tomography, across Greenland towards Baffin Bay. After plate divergence thinned the lithosphere in Baffin Bay around 60 Ma, this could have led to volcanism. Southward increase of divergence would have caused southward flow of plume material, consistent with Baffin Island basalts[2] south of the hotspot track. Comparison with computed hotspot tracks indicates that the corridor across Greenland could have been created by the passage over the plume, heating and thinning the Greenland lithosphere by $\approx 50$ km over a width of $\approx 300$ km[41]. We cannot rule out that this corridor existed prior to the passage of Greenland over the Iceland hotspot. This would require, however, a coincidence of tectonic

structure and plume track by pure chance. If the thin-lithosphere corridor is due to Greenland's passage over the plume at 60-80 Ma, the lithosphere within the corridor could have been $\approx 50$ km thinner[42] at 60 Ma than it is now, after cooling for 60 Myr. It is thus possible that even more hot asthenosphere of plume origin could have reached the west coast of Greenland than predicted by our model.

Compared to previous analytical and numerical models[26, 28, 32, 43] this work takes advantage of key new evidence yielded by new tomography, tomography-derived lithosphere thickness models, and plate reconstructions, as well as improved numerical modelling capabilities. Comparison of detailed model predictions, including the present-day shape of the plume, and the distribution of volcanism in space and time with future seismological, radiometric and geochemical data can provide tests of the model and underlying hypothesis, and may lead to its modification or abandoning.

Many previous tomography models included in a recent compilation[23] show evidence for thin lithosphere in eastern Greenland, near the supposed 60 Ma plume location, but not further west. Recently, thinned lithosphere beneath north-central Greenland has been proposed[44] based on P-wave[45] and S-wave[10] tomographic models, as well as high geothermal flux inferred from ice-penetrating radar and ice core drilling data. The inferred thin lithosphere was linked to its passage over the Iceland plume. The thin-lithosphere corridor seen in our new tomography and lithospheric models is likely to show the complete extent of lithosphere modified by the Iceland plume, as Greenland moved across it. It connects the locations of abundant volcanism at the west and east coasts of Greenland, in contrast with previous tomography models[10, 44, 45], which suggested cold,

thick lithosphere beneath the volcanic areas on Greenland's western coast, difficult to reconcile with voluminous volcanism in those areas. The improvements in tomographic resolution given by our model is mainly due to waveform inversion of a very large dataset of fundamental and higher mode surface waves that constrained it, using all available broadband stations in the region and exploiting the high sensitivity of waveform data to lithospheric structure[34] (see Methods).

Compilations[9,44] show that various proposed fixed and moving hotspot tracks across Greenland are substantially different. Our model considers motion of the Iceland plume from 60 Ma onwards. For earlier times, we assume a fixed plume position. This is presumably a reasonable approximation, as the Iceland plume appears to be a nearly stationary upwelling from the northern tip[46] of the African LLSVP, and numerical models [26,29] yield limited plume motion also after 60 Ma. Importantly, the corresponding hotspot track[29] provides one of the best matches with the East-West corridor across Greenland detected by tomography.

The calculated distribution of volcanism compares well with a crustal thickness map inferred from gravity inversion. However, the thick crust of the Greenland-Iceland ridge[47] and the Faroe-Iceland ridge[48] are not being recreated in their rather narrow aseismic ridge form, and some of the thick crust may be due to continental material, including fragments in the middle of the ocean[17]. With the assumed size (500 km diameter) of the plume head or pulse around 60 Ma, melt is not produced as far into the continent as Scotland and Ireland, where the Tertiary Volcanics occurred around this time. More generally, in our numerical model melt tends to be produced in oceanic regions with thin lithosphere, rather than on neighbouring continents, where volcanics are also

found[40]. Given that the estimates of $5 - 10 \cdot 10^6$ km$^3$, compiled[49] for the volume of volcanics, are very large compared to other LIPs, the 500 km diameter plume head may be considered a conservative estimate; it was more likely larger rather than smaller. Also, a more sheet-like upwelling, extending in a north-south direction, which occurs in geodynamic models[12] at the northern tip of the African LLSVP could help explaining that the extent of simultaneous volcanism around 60 Ma was larger than modelled here.

The immediate cause of the British Tertiary Igneous Province could be lithosphere thinning, triggered by mantle upwelling and laterally transported hot asthenosphere, and due to deformation during the opening of the North Atlantic. The distribution of North Atlantic Igneaous Province (NAIP) volcanism is a good proxy for thin lithospheres. The Irish Sea may have been relatively far from the plume, but locations of NAIP volcanism are scattered between them, and can be taken as fingerprints left by hot asthenosphere flow at the time. Lithosphere thickness variations lead to a pattern of melting that is not radially symmetric. However, the dynamics of the plume itself may lead to viscous fingering[50].

Our model provides support for the single-plume hypothesis and helps to reconcile seemingly contradictory older models: On one hand, it has been proposed that the large volcanic outpourings in the incipient North Atlantic are caused by the initial Iceland plume head. On the other hand, a much earlier origin has been proposed, perhaps linking the Iceland plume to volcanics in Ellesmere and Svalbard. Here we find that even with a plume much older than 60 Ma, volcanism only starts around 60 Ma, when plume material finally finds its way to regions of thin lithosphere east and

west of Greenland. However, before that time, plume material has been accumulated at the base of the lithosphere such that, when melting finally occurs, it is rather massive. This resembles the impinging of a plume head, even though plume material has gradually accumulated over tens of millions of years. In this way, the amounts and distribution of volcanism east of Greenland are in fact rather similar in the cases where a plume head hits at around 62 Ma, and where the plume has continuously existed since much earlier. We suggest that flood basalts do not always represent the arrival of plume heads from the deep mantle[7] but may also occur due to interaction of a plume with a lithosphere[25] with thickness varying in space and time.

## References


1. Pedersen, A., Larsen, L. M., Riisager, P. & Dueholm, K. S. Rates of volcanic deposition, facies changes and movements in a dynamic basin: the Nuussuaq Basin, West Greenland, around the C27n–C26r transition. In Jolley, D. W. & Bell, B. R. (eds.) *The North Atlantic Igneous Province: stratigraphy, tectonics, volcanic and magmatic processes*, vol. 197, 157–181 (Geological Society Special Publication, London, 2002).

2. Stuart, F. M., Solveigh, L.-E., Fitton, J. G. & Ellam, R. M. High $^{3}He/^{4}He$ ratios in picritic basalts from Baffin Island and the role of a mixed reservoir in mantle plumes. *Nature* **424**, 57–59 (2003).

3. Torsvik, T. H., Mosar, J. & Eide, E. A. Cretaceous-Tertiary geodynamics: a North Atlantic exercise. *Geophys. J. Int.* **146**, 850–866 (2001).

4. Graham, D. W. *et al.* Helium isotope composition of the early Iceland mantle plume inferred from the Tertiary picrites of West Greenland. *Earth Planet. Sci. Lett.* **160**, 241–255 (1998).

5. Marty, B., Upton, B. G. J. & Ellam, R. M. Helium isotopes in early Tertiary basalts, north-east Greenland: Evidence for 58 Ma plume activity in the North Atlantic–Iceland volcanic province. *Geology* **26**, 407–410 (1998).

6. Stuart, F. M., Ellam, R. M., Harrop, P. J., Fitton, J. G. & Bell, B. R. Constraints on mantle plumes from the helium isotopic composition of basalts from the British Tertiary Igneous Province. *Earth Planet. Sci. Lett.* **177**, 273–285 (2000).

7. Richards, M. A., Duncan, R. A. & Courtillot, V. E. Flood basalts and hot-spot tracks: plume heads and tails. *Science* **246**, 103–107 (1989).

8. Morgan, W. J. Hotspot tracks and the early rifting of the Atlantic. *Tectonophysics* **94**, 123–139 (1983).

9. Gaina, C., Medvedev, S., Torsvik, T. H. & Werner, S. C. 4D Arctic: A glimpse into the structure and evolution of the Arctic in the light of new geophysical maps, plate tectonics and tomographic models. *Surv. Geophys.* **35**, 1095–1122 (2014).

10. Rickers, F., Fichtner, A. & Trampert, J. The Iceland–Jan Mayen plume system and its impact on mantle dynamics in the North Atlantic region: evidence from full-waveform inversion. *Earth Planet. Sci. Lett.* **367**, 39–51 (2013).

11. Ganerød, M. *et al.* The North Atlantic Igneous Province reconstructed and its relation to the plume generation zone: the Antrim Lava Group revisited. *Geophys. J. Int.* **182**, 183–202 (2010).

12. Steinberger, B. & Torsvik, T. H. A geodynamic models of plumes from the margins of large low shear velocity provinces. *Geochem., Geophys., Geosys.* **13**, Q01W09 (2012).

13. Foulger, G. R. & Anderson, D. L. A cool model for the Iceland hotspot. *J. Volcanol. Geoth. Res.* **141**, 1–22 (2005).

14. Korenaga, J. Mantle mixing and continental breakup magmatism. *Earth Planet. Sci. Lett.* **218**, 1073 (463–473).

15. Ito, G. & van Keken, P. E. Hotspots and melting anomalies. In Schubert, G. & Bercovici, D. (eds.) *Treatise on Geophysics, Volume 7: Mantle Dynamics*, 371–435 (Elsevier, Amsterdam, 2007).

16. Meyer, R., van Wijk, J. & Gernigon, L. North Atlantic Igneous Province: A review of models for its formation. *GSA Special Paper* **430**, 525–552 (2007).

17. Torsvik, T. H. *et al.* Continental crust beneath southeast Iceland. *P. Natl. Acad. Sci. USA* **112**, E1818–E1827 (2015).

18. Abdelmalak, M. M. *et al.* The ocean-continent transition in the mid-Norwegian margin: Insight from seismic data and an onshore Caledonian field analogue. *Geology* **43**, 1011–1014 (2015).

19. Torsvik, T. H. & Cocks, L. R. M. *Earth History and Paleogeography* (Cambridge University Press, 2017).

20. Wolfe, C. J., Bjarnason, I. T., VanDecar, J. C. & Solomon, S. C. Seismic structure of the Iceland mantle plume. *Nature* **385**, 245–247 (1997).

21. Bijwaard, H. & Spakman, W. Tomographic evidence for a narrow whole mantle plume below Iceland. *Earth Planet. Sci. Lett.* **166**, 121–126 (1999).

22. French, S. W. & Romanowicz, B. Broad plumes rooted at the base of the Earth's mantle beneath major hotspots. *Nature* **525**, 95–99 (2015).

23. Steinberger, B., Spakman, W., Japsen, P. & Torsvik, T. H. The key role of global solid Earth processes in the late Cenozoic intensification of Greenland glaciation. *Terra Nova* **27**, 1–8 (2015).

24. Morgan, W. J. Rodriguez, Darwin, Amsterdam, . . . , A second type of Hotspot Island. *J. Geophys. Res.* **83**, 5355–5360 (1978).

25. Sleep, N. H. Lateral flow and ponding of starting plume material. *J. Geophys. Res.* **102**, 10001–10012 (1997).

26. Mihálffy, P., Steinberger, B. & Schmeling, H. The effect of the large-scale mantle flow field on the Iceland hotspot track. *Tectonophys.* **447**, 5–18 (2008).

27. Bjarnason, I. T., Silver, P. G., Rümpker, G. & Solomon, S. C. Shear wave splitting across the Iceland hot spot: Results from the ICEMELT experiment. *J. Geophys. Res.* **107**, 2382 (2002).

28. Ito, G., Dunn, R. & Li, A. The origin of shear wave splitting beneath Iceland. *Geophys. J. Int.* **201**, 1297–1312 (2015).

29. Doubrovine, P. V., Steinberger, B. & Torsvik, T. H. Absolute plate motions in a reference frame defined by moving hot spots in the Pacific, Atlantic, and Indian oceans. *J. Geophys. Res.* **117**, B09101 (2012).

30. O'Neill, C., Müller, R. D. & Steinberger, B. On the uncertainties in hotspot reconstructions, and the significance of moving hotspot reference frames. *Geochem., Geophys., Geosys.* **6**, Q04003 (2005).

31. Lawver, L. A. & Müller, R. D. Iceland hotspot track. *Geology* **22**, 311–314 (1994).

32. Vink, G. E. A hotspot model for Iceland and the Vøring Plateau. *J. Geophys. Res.* **89**, 9949–9959 (1984).

33. Morgan, W. J. Hotspot tracks and the opening of the Atlantic and Indian oceans. In Emiliani, C. (ed.) *The Sea Vol. 7 The Oceanic Lithosphere*, 443–487 (Wiley, New York, 1981).

34. Lebedev, S., Schaeffer, A. J., Fullea, J. & Pease, V. Seismic tomography of the Arctic region: Inferences for the thermal structure and evolution of the lithosphere. In Pease, V. & Coakley, B. (eds.) *Circum-Arctic Lithosphere Evolution*, vol. 460, 419–440 (Geological Society Special Publications, London, 2018).

35. Torsvik, T. H., Steinberger, B., Gurnis, M. & Gaina, C. Plate tectonics and net lithosphere rotation over the past 150 My. *Earth Planet. Sci. Lett.* **291**, 106–112 (2010).

313 36. Pourpoint, M., Anandakrishnan, S. A. & Ammon, C. J. Highresolution rayleigh wave group
314 velocity variation beneath greenland. *J. Geophys. Res.* **123**, 1516–1539 (2018).

315 37. Mordret, A. Uncovering the iceland hotspot track beneath greenland. *J. Geophys. Res.* (2018).

316 38. White, R. & McKenzie, D. Magmatism at rift zones: The generation of volcanic continental
317 margins and flood basalts. *J. Geophys. Res.* **94**, 7685–7729 (1989).

318 39. Gassmöller, R., Dannberg, J., Bredow, E., Steinberger, B. & Torsvik, T. H. Major influence
319 of plume-ridge interaction, lithosphere thickness variations and global mantle flow on hotspot
320 volcanism - the example of Tristan. *Geochem., Geophys., Geosys.* **17**, 1454–1479 (2016).

321 40. Bredow, E., Steinberger, B., Gassmöller, R. & Dannberg, J. How plume-ridge interaction
322 shapes the crustal thickness pattern of the Réunion hotspot track. *Geochem., Geophys.,*
323 *Geosys.* **18**, 2930–2948 (2017).

324 41. Yang, T. & Leng, W. Dynamics of hidden hotspot tracks beneath the continental lithosphere.
325 *Earth Planet. Sci. Lett.* **401**, 294–300 (2014).

326 42. Yuan, X. *et al.* Seismic structure of the lithosphere beneath NW Namibia: Impact of the
327 Tristan da Cunha mantle plume. *Geochem., Geophys., Geosys.* **18**, 125–141 (2017).

328 43. Beniest, A., Koptev, A., Leroy, S., Sassi, W. & Guichet, X. Two-branch break-up systems by
329 a single mantle plume: Insights from numerical modeling. *Geophys. Res. Lett.* **44**, 9589–9597
330 (2017).

331 44. Rogozhina, I. *et al.* Melting at the base of the Greenland Ice Sheet explained by Iceland
332 hotspot history. *Nat. Geosci.* **9**, 366–369 (2016).

333 45. Jakovlev, A. V., Bushenkova, N. A., Koulakov, I. Y. & Dobretsov, N. L. Structure of the upper
334 mantle in the circum-Arctic region from regional seismic tomography. *Russ. Geol. Geophys.*
335 **22**, 963–971 (2012).

336 46. Lekic, V., Cottaar, S., Dziewonski, A. & Romanowicz, B. Cluster analysis of global lower
337 mantle tomography: a new class of structure and implications for chemical heterogeneity.
338 *Earth Planet. Sci. Lett.* **357–358**, 68–77 (2012).

339 47. Holbrook, W. S. *et al.* Mantle thermal structure and active upwelling during continental
340 breakup in the North Atlantic. *Earth Planet. Sci. Lett.* **190**, 251–266 (2001).

341 48. Smallwood, J. R., Staples, R. K., Richardson, K. R. & White, R. S. Crust generated above
342 the Iceland mantle plume: From continental rift to oceanic spreading center. *J. Geophys. Res.*
343 **104**, 22885–22902 (1999).

344 49. Storey, M., Duncan, R. A. & Tegner, C. Timing and duration of volcanism in the North Atlantic
345 Igneous Province: Implications for geodynamics and links to the Iceland hotspot. *Chem. Geol.*
346 **241**, 264–281 (2007).

347 50. Schoonman, C. M., White, N. J. & Pritchard, D. Radial viscous fingering of hot asthenosphere
348 within the Icelandic plume beneath the North Atlantic Ocean. *Earth Planet. Sci. Lett.* **468**, 51–
349 61 (2017).

**Corresponding author:** Correspondence and requests for materials should be addressed to B.S. (email: bstein@gfz-potsdam.de).

**Acknowledgements** The geodynamic models were computed with the open-source software ASPECT (*http://aspect.dealii.org*) and performed with resources provided by the North-German Supercomputing Alliance (HLRN). We thank Juliane Dannberg, Simon Williams, Nicky White and Ingi Bjarnason for comments and suggestions. This publication has emanated from research supported in part by research grants from Science Foundation Ireland (SFI) under grant number 13/CDA/2192 and grant number 13/RC/2092, co-funded under the European Regional Development Fund and by iCRAG industry partners. B.S. and T.H.T. also acknowledge support from the Research Council of Norway, through its Centre of Excellence scheme, project number 223272 (CEED).

**Author Contributions** S.L. and B.S. conceived the paper. B.S. wrote the paper, with help from all other authors. E.B. performed the computations with ASPECT. A.S. and S.L. provided tomography and lithosphere thickness models. T.H.T. provided plate reconstructions and data on the distribution of volcanics. All authors jointly contributed to discussions.

**Competing interests** The authors declare that they have no competing interests.

**Supplementary information** is linked to the online version of the paper

Figure 1: Main volcanic facies linked to North Atlantic Igneous Province (NAIP), Iceland and North Atlantic opening. Site locations for dated NAIP magmatism shown as color-coded filled circles[3,17]. BI, Baffin Island; COB, Transition between continental and oceanic crust; JMMC, Jan Mayen microcontinent; SDRs, seaward dipping reflectors. Volcanic facies drawn from many sources, including ref.[18]. Inset histogram based on a compilation[17] of 383 isotope ages from NAIP, mainly $^{40}Ar/^{39}Ar$ and K/Ar ages, with 3% high-precision U/Pb ages[19], 62.6 Ma (Antrim basalt in Ireland) to 55.5 Ma (Skaergaard intrusion in East Greenland), 55.6 and 56.3 Ma (magmatic sills in the Vøring area, offshore mid-Norway).

Figure 2: Lithosphere thickness at 60 Ma and present-day. Left: Continental lithosphere thickness based on Arctic tomography model AMISvArc[34] and backward-rotation using a plate reconstruction[29]; oceanic regions based on sea floor ages (see Methods). White lines for plate boundaries, golden star for plume position[29]. Right: Lithosphere thickness from tomography[34] only. Reconstructed plume track on Greenland[29,35] is shown for 120-60 Ma. As mantle flow and hence plume motion become increasingly uncertain back in time, we assume a fixed hotspot[8,33] for $>$ 60 Ma. Regions labelled Ellesmere and Svalbard are parts of the High Arctic Large Igneous Province[19].

Figure 3: Arctic tomography model AMISvArc[34] beneath Greenland and surroundings. The reference value of vertically-polarized S-wave speed in the mantle is 4.38 km/s. This value and deviations from it are at the reference period 50 s. Plume track as in Fig. 2. Fig. S4 shows resolution tests, indicating that the East-West reduced-velocity channel is well-resolved, and would not manifest as an artefact without actual reduced seismic velocities. Relatively low seismic velocities in this channel are confirmed by recent regional tomography studies[36, 37], using smaller datasets but with data from most of the new stations in Greenland that were used to construct AMISvArc.

Figure 4: Numerical model (Model115Ma) of the Iceland plume, represented by the 100 K isosurface colored according to melt fraction. The plume is initiated at 115 Ma and we show two representative time frames in oblique and top view. Red lines are plate boundaries, green arrows represent absolute plate velocities[29]. The top left panel also illustrates side boundary conditions, based on plate motions and global mantle flow (see Methods). The complete model development is also shown in a supplementary movie.

Figure 5: Computed excess crustal thickness produced by the plume in Model115Ma (left) and crustal thickness based on gravity inversion[17] (right). Melt that is generated is immediately extracted to the surface and rotated to its present location according to the plate reconstruction[29,35]. The difference between two model runs with plume and without is shown. Yellow stars connected with white line show the 60-0 Ma Iceland plume track[29,35] (modified in left panel, as described in Methods). Red line is the North Atlantic spreading ridge, blue lines are the Continent-Ocean transition zones[17]. IGR = Iceland Greenland Ridge; JM = Jan Mayen; JMM = Jan Mayen Microcontinent.

Figure 6: Computed plume-related melt produced in different time intervals, represented as present-day crustal thickness contribution (as in Fig. 5). In Model115Ma the plume has been displaced 300 km westward at 70-60Ma (see Methods). Apart from some melting in Baffin Bay and Labrador Sea, results for the two models are rather similar after 55 Ma, hence only Model115Ma results are shown for these later times. Corresponding plume location relative to Greenland at 60, 50, 40 and 30 Ma is shown as yellow stars. Color-coded dots show dated volcanics in the same time intervals for an updated compilation[3,17].

## Methods

**Geodynamic model** Apart from minor modifications, the work flow essentially follows the steps described in Bredow et al.[40]: The computations are carried out with the mantle convection code ASPECT[51,52] in a 3-D Cartesian box of dimensions length x width x height = 3300 x 3300 x 660 km from an inital time (120 Ma or 80 Ma) until present. The temperature field is prescribed at first to take into account the reconstructed lithosphere thickness distribution at the initial time and later as time-dependent boundary conditions. Velocity boundary conditions at the surface and the upper 200 km of the side boundaries simulate plate motions and are derived from a plate reconstruction model (see next subsection). The global flow surrounding the model domain is derived from a global mantle flow model (see below) and prescribed at the side boundaries below 200 km and at the base of the model box. All boundary conditions are time-dependent and prescribed at all times. Since due to the transformation from spherical to Cartesian coordinates the global flow and plate velocities do not exactly correspond to each other, they are smoothly interpolated at 200 km depth at the side boundaries. In addition, plume inflow at the bottom of the box is prescribed at a location inferred from a global model (see below). We use a plume head radius of 250 km, an excess temperature of 300 K and an inflow velocity of 20 cm/yr (comparable with recent models of the Tristan da Cunha[39] and Réunion[40] mantle plumes). The plume tail has an excess temperature of 250 K in agreement with literature estimates, which range between 186 K and 300 K[53–56], a radius of 140 km and an inflow velocity of 6 cm/yr. These values result in a pure plume buoyancy flux of approximately 1150 kg/s, which is heightened by the global flow to a total range between 1250 kg/s and 2000 kg/s, in accordance with estimated values[54,55]. To maintain conservation of mass,

every simulation runs twice and the net mass flux from the first simulation is used to correct the velocity boundary conditions for the second simulation. This correction is rather small and results with and without are visually very similar.

Global mantle flow is computed in terms of spherical harmonics[57,58], for a given 3-dimensional mantle density structure, radial viscosity profile, prescribed surface plate motions (see next subsection) and a free-slip core-mantle boundary (CMB). These plate motions include a net rotation component, and in order to maintain this surface net rotation, but with strongly reduced net rotation in the deep mantle, we use a fixed CMB for the toroidal degree one flow component only. Density anomalies are backward advected[59] in the flow field to 68 Ma, and kept constant before that. The global flow model for present-day has been described in[60]: The density model is based on surface wave tomography model[61] in the upper 200 km and the 2010 update of a whole-mantle model[62] below that. For most of the mantle, we use a thermal scaling to density (Figure 3A of Steinberger[60]), however, given that both continental lithosphere and the LLSVP of the lowermost mantle are likely chemically distinct, we use a different scaling there: Inside the continental lithosphere (see subsection below) shallower than 150 km depth we instead set the density anomaly to a constant 0.2%. Inside the LLSVPs, a density anomaly of 1.2 % has been added. LLSVPs are assumed to be in the lowermost 300 km of the mantle wherever seismic anomalies are more than 1 % negative. For viscosity, we use the red profile in Figure 3A of Steinberger[60], with viscosity increasing from $\approx 10^{20}$ Pas in the asthenosphere to nearly $10^{23}$ Pas in the lower mantle, but again decreasing to below $10^{21}$ Pas at the CMB. In contrast to the global flow model, our regional model considers temperature-dependent viscosity, which leads to lower sublithospheric viscosity in the

vicinity of the plume (see Fig. S3).

The motion of the plume is computed following the method first developed by Steinberger and O'Connell[59] with parameters as in Steinberger et al.[63]: The plume conduit is assumed to be initially (at 60 Ma) vertical and subsequently distorted in, but also buoyantly rising through mantle flow. A vertical plume conduit at 60 Ma corresponds to the assumption that the plume conduit was established by a plume head rising comparatively fast through the mantle. Alternatively, in case a pre-existing plume is assumed, it may represent a large pulse rising through, and straightening out the conduit. In this case, we had used an earlier tomography model[64], and somewhat different viscosity and scaling from seismic velocity to density[65] (model 2b of that paper; scaling from seismic velocity to density reduced by a factor 0.5 in the upper 220 km) to compute flow. Since this model fits the geoid well, we expect that it gives a realistic prediction of large-scale flow in the lower mantle, which is relevant for plume motion. In contrast, the model used to compute inflow and outflow at the boundaries of the box gives a better prediction of dynamic topography, therefore we expect that it realistically includes more details of upper mantle flow. From this global model of plume motion, the plume position at depth 660 km is extracted to prescribe the plume influx into the regional model box. Since the regional model is initiated at 64 Ma to allow for rising of the plume head, a constant position is assumed 64-60 Ma. In Model115Ma, it is kept in the same position as the reference case until 80 Ma, is 300 km further west 70-60 Ma, 150 km further west and 100 km further south at 55 Ma, and in the same position as the reference case from 50 Ma, with linear interpolation. This is meant to compensate for a kink in the plate motion model, and should mimic the case where the plume moves in the same way after 60 Ma and is

fixed before that, with a smoothed-out plate motion model. In this way, the speed of Greenland relative to the plume in the 80-70 Ma interval is reduced to somewhat more than half, instead of by modifying absolute plate motion[29,35], approximately within uncertainties (see also Fig. S2). Given the increasing uncertainties in models of mantle flow and plume motion further back in time, we regard it as justified to revert to a model meant to represent a fixed plume before 60 Ma.

Melting in the geodynamic model depends on pressure and temperature and is calculated based on the parametrization for batch melting of anhydrous peridotite[66]. In a postprocessing routine, the melt produced in each time step is instantly extracted to the surface and moved with the according plate motions. As in Bredow et al.[40], we employ a dehydration rheology and a depletion buoyancy in our models.

**Plate reconstructions** Where the plume was located relative to the overlying lithosphere depends on both plate motions and the motion of the plume in the same reference frame. Here we adopt absolute plate motions in a global moving hotspot reference frame (GMHRF)[29]. This reference frame is aimed at optimally fitting geometry of and age progression along several hotspot tracks while taking plume motion into account. Since the Iceland plume does not show a classical hotspot track, it is not included in devising this reference frame. Hotspot reference frames that are only for the Indo-Atlantic hemisphere[30] somewhat differ from a global reference frame that also takes hotspot tracks in the Pacific[29] into account. In particular, around 60 Ma, in an Indo-Atlantic reference frame the Iceland plume is located further west relative to Greenland – beneath central to eastern Greenland rather than beneath its eastern coast.

Relative plate motions and plate boundaries in 10 Myr intervals are initally from Torsvik et al.[35], but plate boundaries are transferred with a routine described in that paper to the GMHRF[29]. Plate motions are converted to cartesian coordinates corresponding to the center of the model box at 17° W 64° N. A Lambert azimuthal equal-area projection is used to convert plate boundaries and the models of large-scale mantle flow, plume motion and lithosphere thickness described in this methods section to box coordinates. Interpolation of plate boundaries from 10 Myr intervals to 1 Myr is done using a semi-automated procedure where essentially corresponding features in the plate boundaries (ridge segments, transform faults) are identified and matched by eye, and then automatically interpolated.

**Mantle Tomography model AMISvArc** AMISvArc is a new upper-mantle shear-wave speed model of the circum-Arctic region[34]. It is constructed as a global model using the same methodology and similar datasets as the recently published models Sl2016svA[67], SL2013NA[68], and SL2013sv[61], but with substantially more data in the Arctic.

The inversion procedure comprises three steps. First, the Automated Multimode Inversion of surface and S wave-forms (AMI[69]) is applied to a pre-processed dataset of displacement seismograms. AMI performs accurate, automated processing of massive volumes of broadband waveform data, applying elaborate case-by-case selection of time-frequency windows and relative weighting of the fundamental and higher mode arrivals (S and multiple-S waves), while enforcing a strict misfit criterion across all windows. Each successfully fit seismogram yields a set of linear equations with uncorrelated uncertainties that describe 1D perturbations in S- and P-wave velocities within approximate finite-width sensitivity volumes between the source and receiver, with respect

to a global 3D reference model. The 3D reference model comprises the crustal model CRUST2[70] smoothed across its $2^\circ$ cell boundaries and augmented with global topographic and bathymetric databases and, beneath the Moho, the global 1D reference model AK135[71], recomputed at a reference period of 50 s. Crustal structure, i.e., the deviations from the 3D reference model at the 3-4 crustal grid knots (depths of 7, 20, 36 and 56 km) are solved for in the inversion, instead of adopting the common assumption of fixed crustal structure or of crustal corrections. Errors in the Moho depth are compensated primarily by changes in the lower-crustal and uppermost mantle velocities [72].

In the second step, linear equations from all seismograms successfully fit by AMI (for a detailed overview of the results of waveform fitting, see Schaeffer and Lebedev[61]) are combined into a single linear system and solved for the 3D distribution in isotropic P- and S-wave speeds and $2\Psi$ azimuthal anisotropy of S-wave velocity[67], with respect to a modified 3D reference model that now comprises CRUST2 in the crust and the 1D upper mantle average taken from our own tomography[73]. The inversion is performed with the LSQR method[74], subject to regularization (norm damping, lateral and vertical smoothing).

The third step of the procedure is the outlier analysis[61,73] aimed at selecting only the most mutually consistent seismogram fits for the final model. This analysis exploits the substantial redundancy of the dataset in order to remove the data most affected by errors (coming from event mislocations, etc). The starting dataset used in constraining AMISvArc includes waveform fits from the models SL2013NA and SL2013sv, and additional, recently recorded or recently made available, data from stations in the Arctic region[34]. The total dataset includes more than one million

vertical component seismograms successfully fit using AMI, recorded at more than 4600 stations globally. Outlier analysis was used to select a subset of 830,000 most mutually consistent waveform fits for an initial inversion; a final step of outlier analysis reduced the number of waveform fits to 817,200.

**Lithosphere Thickness** Present-day lithosphere thickness on continents is computed based on tomography model AMISvArc[34] (see previous section) using the same procedure and parameters as in the reference case of Steinberger[60]. Conceptually, this model is based on the assumption that, in the global average, the temperature profile in the top thermal boundary layer of the mantle, which includes the lithosphere, follows an error function profile. It is further considered that compositional anomalies also contribute to seismic velocity anomalies. We assume that, on global average, this additonal contribution has a depth dependence that also follows an error function profile with the same scaling depth. Further, we assume these compositional anomalies only occur inside the lithosphere and not at the LAB. Under these assumptions, we can now convert seismic velocity anomalies to absolute temperature, and we set the LAB to a constant temperature such that the temperature difference between LAB and surface is 84.3%=erf(1) of the total difference between (adiabatic) mantle potential temperature and surface temperature. Scaling depth of the error function and the compositional contribution to the global average of seismic velocity are two free parameters in this model, and they are adjusted (for a given tomography model) such that the oceanic depth versus age curve (assuming isostasy) is optimally matched.

Present-day continental lithosphere thickness grids are then assigned to four different plates North America, Greenland, Jan Mayen and Eurasia. Lithosphere may become thicker with age,

or thinner due to the influence of the plume[44,75,76]. However, here we simply backward-rotate continents, using our reconstruction[29], for the respective plates. In the oceans (wherever the age grid[77] is defined), present-day lithosphere thickness is computed from sea floor age with a diffusivity $8 \cdot 10^{-7}\mathrm{m}^2\mathrm{s}^{-1}$. Lithosphere thickness in the past is again determined with backward-rotation, but also taking into account that age and hence thickness was less at past times. Past lithosphere thickness determined in this way is applied to the numerical model at the inital time (either 80 Ma or 120 Ma) for the whole box, but afterwards only at the sides, where material moves into the box. Elsewhere, the thickness of lithosphere that either moves into the box or gets created at the ridge is computed self-consistently, such that in effect the lithosphere thickness in our numerical model is very similar to, but not exactly the same as in Fig. 2 left.

**Code Availability** The version of ASPECT we used to run our models is available online (*https://github.com/ebredow/aspect/tree/reunion_plume_model*).

**Data Availability** All of the input files that are required to reproduce this study are provided upon request.

## Methods References


51. Bangerth, W., Dannberg, J., Gassmöller, R., Heister, T. *et al.* ASPECT*: Advanced Solver for Problems in Earths ConvecTion, User Manual* (2017).

52. Kronbichler, M., Heister, T. & Bangerth, W. High accuracy mantle convection simulation through modern numerical methods. *Geophys. J. Int.* **191**, 12–29 (2012).

532 53. Putirka, K. Excess temperatures at ocean islands: Implications for mantle layering and con-
533 vection. *Geology* **36**, 283–286 (2008).

534 54. Sleep, N. Hotspots and mantle plumes: Some phenomenology. *J. Geophys. Res.* **95**, 6715–
535 6736 (1990).

536 55. Schilling, J.-G. Fluxes and excess temperatures of mantle plumes inferred from their interac-
537 tion with migrating mid-ocean ridges. *Nature* **352**, 397–403 (1991).

538 56. Spice, H. E., Fitton, J. G. & Kirstein, L. A. Temperature fluctuation of the Iceland mantle
539 plume through time. *Geochem., Geophys., Geosys.* **17**, 243–254 (2016).

540 57. Hager, B. H. & O'Connell, R. J. Kinematic models of large-scale flow in the Earth's mantle.
541 *J. Geophys. Res.* **84**, 1031–1048 (1979).

542 58. Hager, B. H. & O'Connell, R. J. A simple global model of plate dynamics and mantle convec-
543 tion. *J. Geophys. Res.* **86**, 4843–4867 (1981).

544 59. Steinberger, B. & O'Connell, R. J. Advection of plumes in mantle flow; implications on
545 hotspot motion, mantle viscosity and plume distribution. *Geophys. J. Int.* **132**, 412–434 (1998).

546 60. Steinberger, B. Topography caused by mantle density variations: Observation-based estimates
547 and models derived from tomography and lithosphere thickness. *Geophys. J. Int.* **205**, 604–621
548 (2016).

549 61. Schaeffer, A. J. & Lebedev, S. Global shear speed structure of the upper mantle and transition
550 zone. *Geophys. J. Int.* **194**, 417–449 (2013).

551 62. Grand, S. P. Mantle shear-wave tomography and the fate of subducted slabs. *Phil. Trans. R.*
552 *Soc. Lond. A* **360**, 2475–2491 (2002).

553 63. Steinberger, B., Sutherland, R. & O'Connell, R. J. Prediction of Emperor-Hawaii seamount
554 locations from a revised model of global plate motion and mantle flow. *Nature* **430**, 167–173
555 (2004).

556 64. Becker, T. W. & Boschi, L. A comparison of tomographic and geodynamic mantle models.
557 *Geochem., Geophys., Geosys.* **3** (2002).

558 65. Steinberger, B. & Calderwood, A. Models of large-scale viscous flow in the Earth's mantle
559 with constraints from mineral physics and surface observations. *Geophys. J. Int.* **167**, 1461–
560 1481 (2006).

561 66. Katz, R. F., Spiegelman, M. & Langmuir, C. H. A new parameterization of hydrous mantle
562 melting. *Geochem., Geophys., Geosys.* **4**, 1073 (2003).

563 67. Schaeffer, A. J., Lebedev, S. & Becker, T. W. Azimuthal seismic anisotropy in the Earth's
564 upper mantle and the thickness of tectonic plates. *Geophys. J. Int.* **207**, 901–933 (2016).

565 68. Schaeffer, A. J. & Lebedev, S. Imaging the North American continent using waveform inver-
566 sion of global and USArray data. *Earth Planet. Sci. Lett.* **402**, 26–41 (2014).

567 69. Lebedev, S., Nolet, G., Meier, T. & van der Hilst, R. D. Automated multimode inversion of
568 surface and S waveforms. *Geophys. J. Int.* **162**, 951–964 (2005).

569 70. Bassin, C., Laske, G. & Masters, G. The current limits of resolution for surface wave tomog-
570 raphy in North America. *EOS, Trans Am. Geophys. Un.* **81**, F897 (2000).

571 71. Kennett, B. L. N., Engdahl, E. R. & Buland, R. Constraints on seismic velocities in the Earth
572 from traveltimes. *Geophys. J. Int.* **122**, 108–124 (1995).

573 72. Lebedev, S., Adam, J. M.-C. & Meier, T. Mapping the Moho with seismic surface waves: A
574 review, resolution analysis, and recommended inversion strategies. *Tectonophysics "Moho", Special Issue* **609**, 377–394 (2013).

576 73. Lebedev, S. & van der Hilst, R. D. Global upper-mantle tomography with the automated
577 multimode inversion of surface and s-wave forms. *Geophys. J. Int.* **173**, 505–518 (2008).

578 74. Paige, S. & Saunders, C. C. LSQR: An algorithm for sparse linear equations and sparse least
579 squares. *ACM T. Math. Software* **8**, 43–71 (1982).

580 75. Detrick, R. S. & Crough, S. T. Island subsidence, hot spots, and lithospheric thinning. *J.*
581 *Geophys. Res.* **83**, 1236–1244 (1978).

582 76. Chu, R., Leng, W., Helmberger, D. V. & Gurnis, M. Hidden hotspot track beneath the eastern
583 United States. *Nat. Geosci.* **6**, 963–966 (2013).

584 77. Müller, R. D., Sdrolias, M., Gaina, C. & Roest, W. R. Age, spreading rates, and spreading
585 asymmetry of the world's ocean crust. *Geochem., Geophys., Geosys.* **9**, Q04006 (2008).

586 78. Torsvik, T. H. *et al.* Phanerozoic polar wander, paleogeography and dynamics. *Earth Sci. Rev.*
587 **114**, 325–368 (2012).

588 79. Matthews, K. J. *et al.* Global plate boundary evolution and kinematics since the late Paleozoic.
589 *Global Planet. Change* **146**, 226–250 (2016).

590 80. Torsvik, T. H., Müller, R. D., Van der Voo, R., Steinberger, B. & Gaina, C. Global plate motion
591 frames: Toward a unified model. *Rev. Geophys.* **46**, RG3004 (2008).

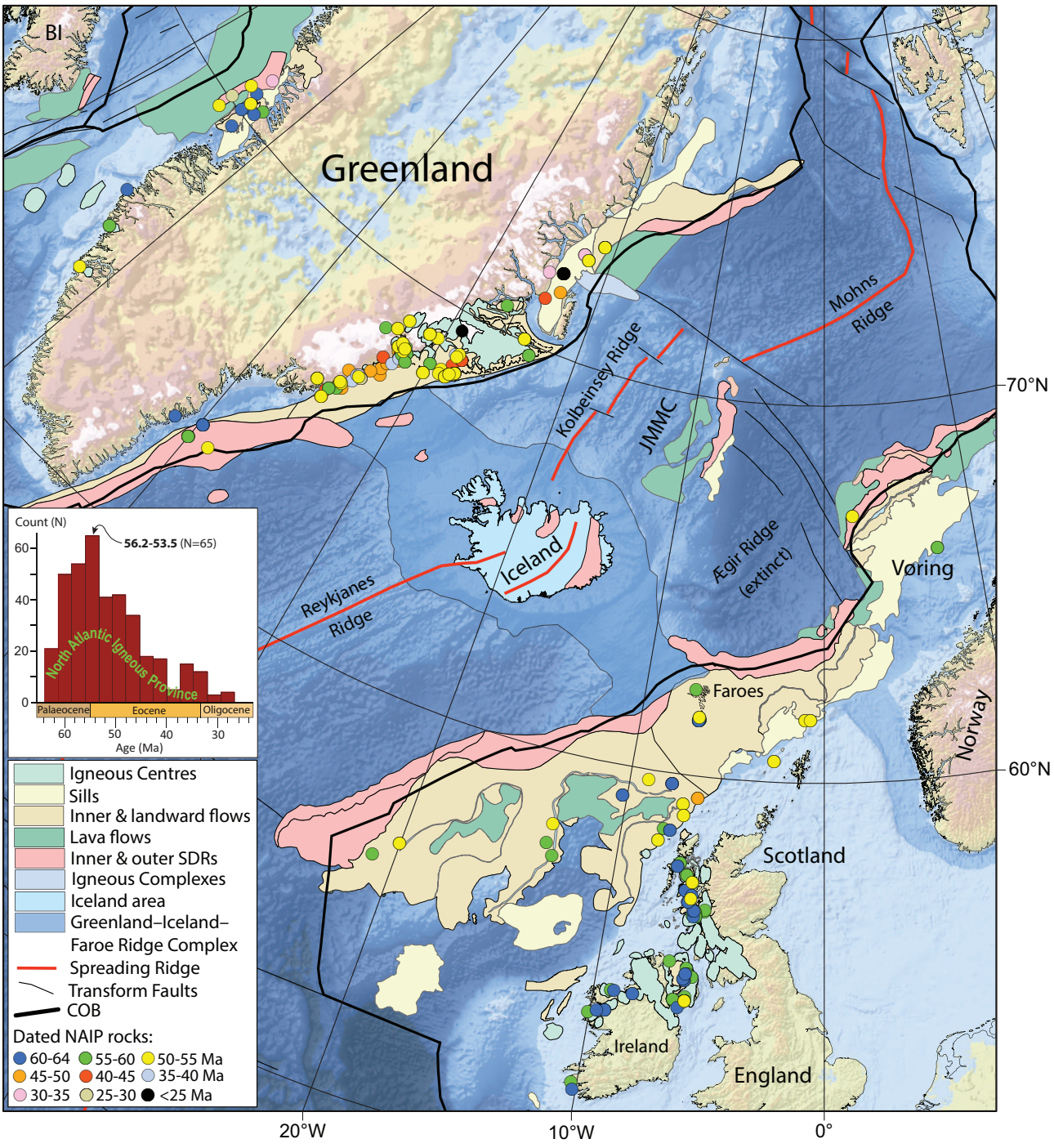
BI
Greenland
Mohns Ridge
Kolbeinsey Ridge
JMMC
70°N
Iceland
Ægir Ridge (extinct)
Reykjanes Ridge
Vøring
Faroes
Norway
60°N
Scotland
Ireland
England
20°W
10°W
0°
Count (N)
56.2-53.5 (N=65)
North Atlantic Igneous Province
Palaeocene
Eocene
Oligocene
Age (Ma)
Igneous Centres
Sills
Inner & landward flows
Lava flows
Inner & outer SDRs
Igneous Complexes
Iceland area
Greenland–Iceland–Faroe Ridge Complex
Spreading Ridge
Transform Faults
COB
Dated NAIP rocks:
60-64
55-60
50-55 Ma
45-50
40-45
35-40 Ma
30-35
25-30
<25 Ma

Figure 1

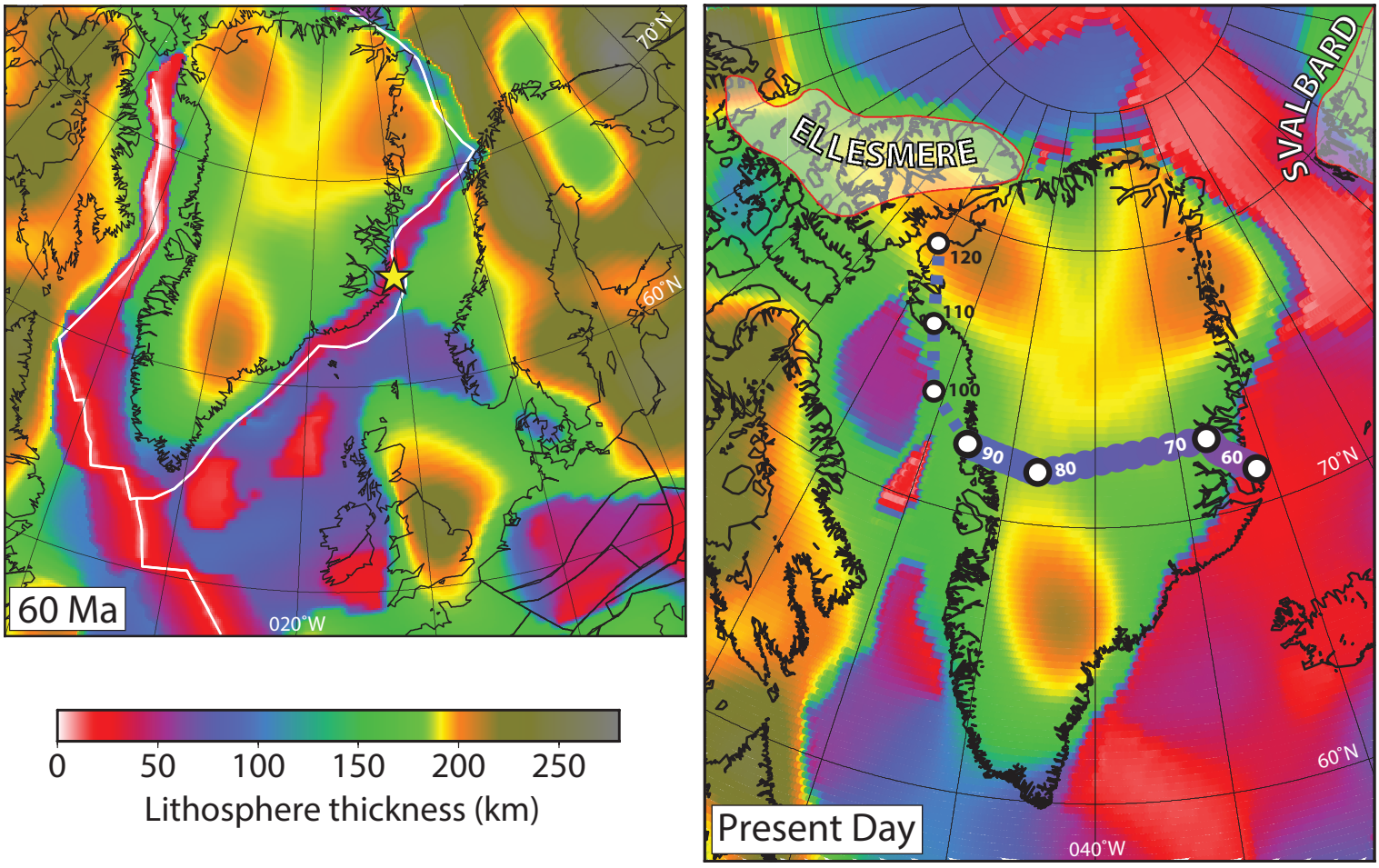
70°N
60°N
60 Ma
020°W
0
50
100
150
200
250
Lithosphere thickness (km)
ELLESMERE
SVALBARD
120
110
100
90
80
70
60
70°N
60°N
Present Day
040°W

Figure 2

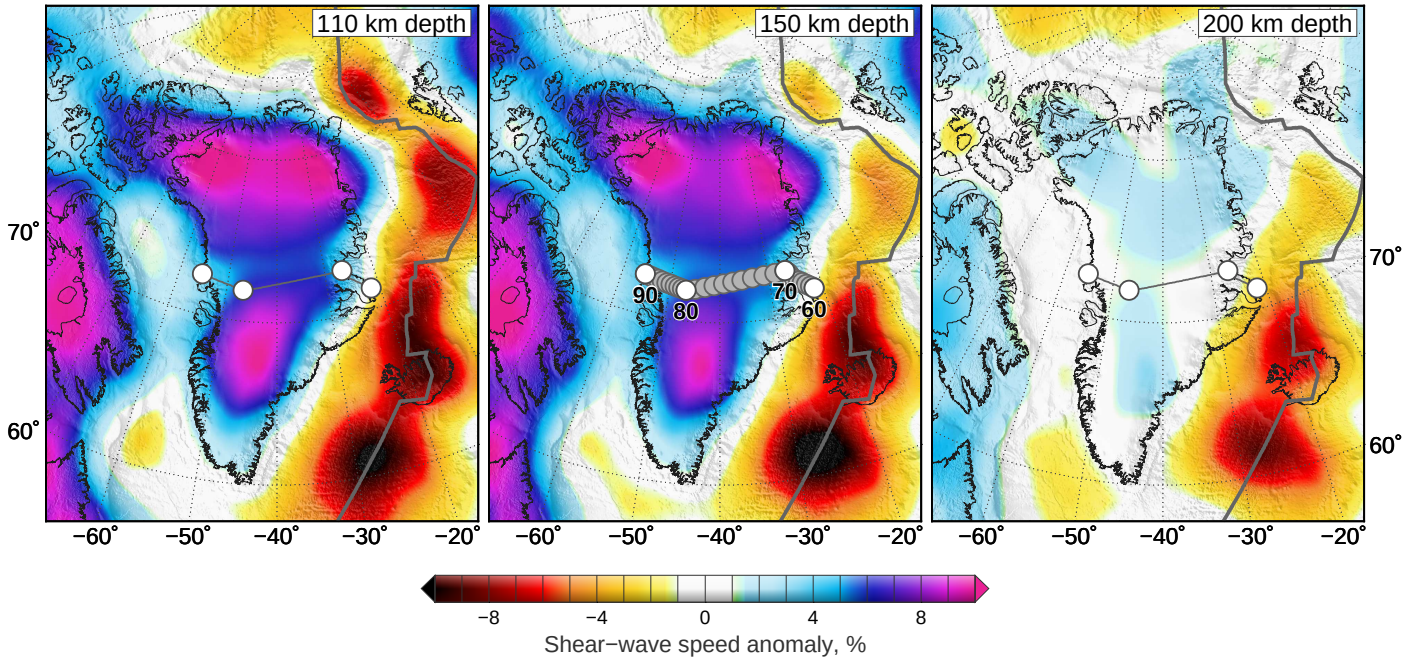
110 km depth
150 km depth
200 km depth
70˚
60˚
−60˚
−50˚
−40˚
−30˚
−20˚
90
80
70
60
−8
−4
0
4
8
Shear−wave speed anomaly, %

Figure 3

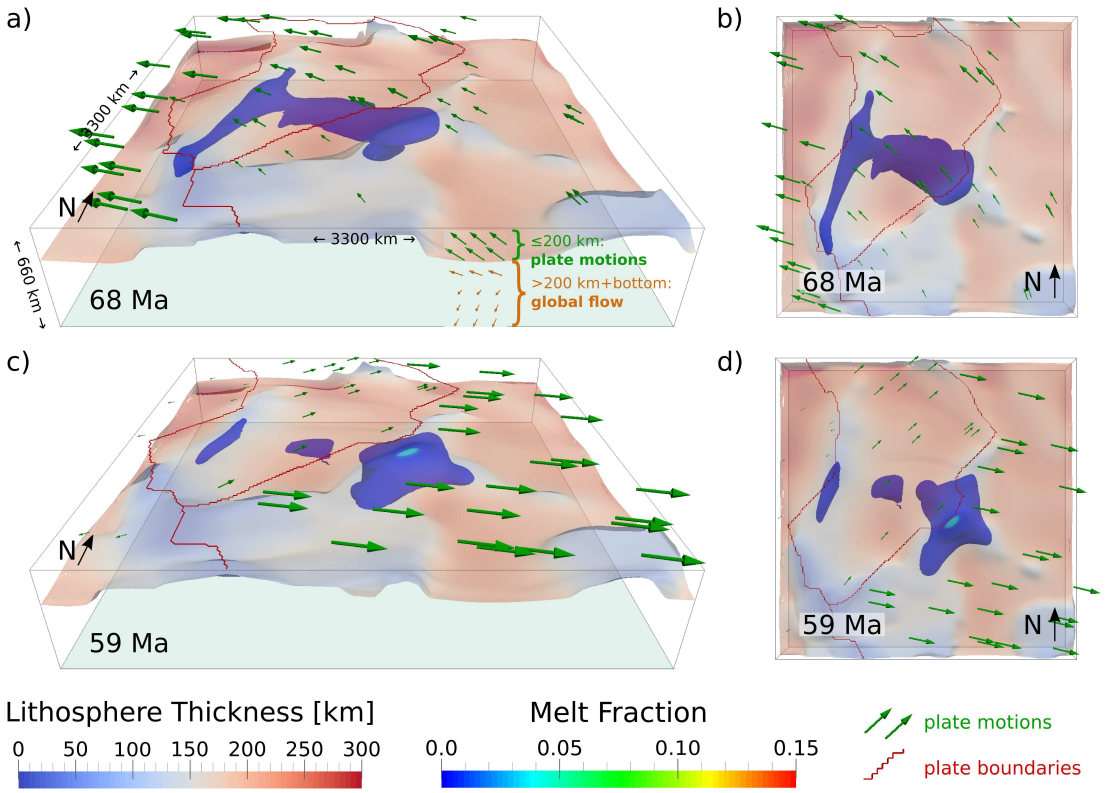


Figure 4

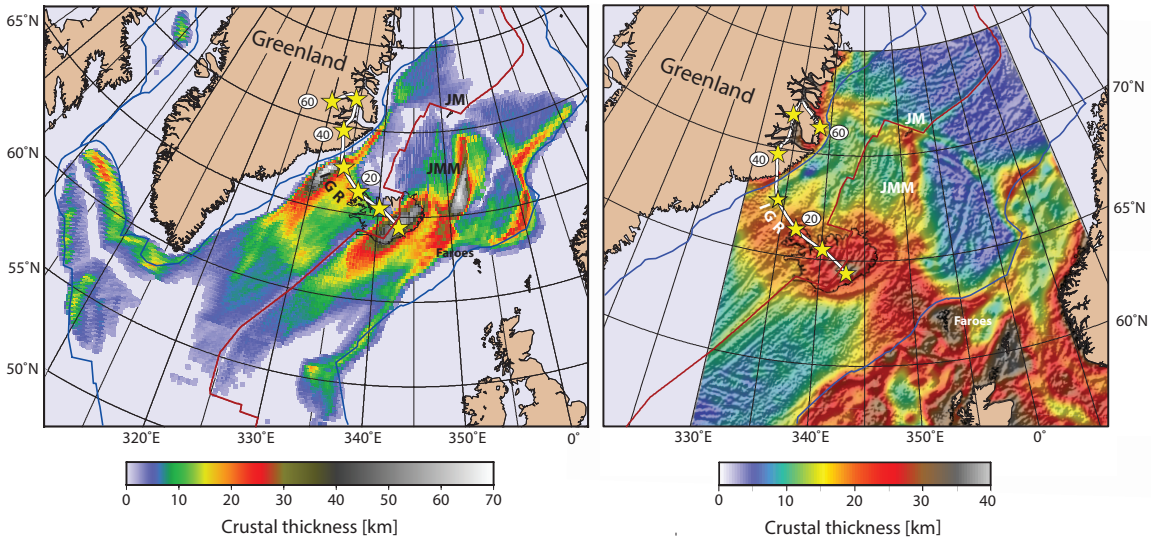


Figure 5

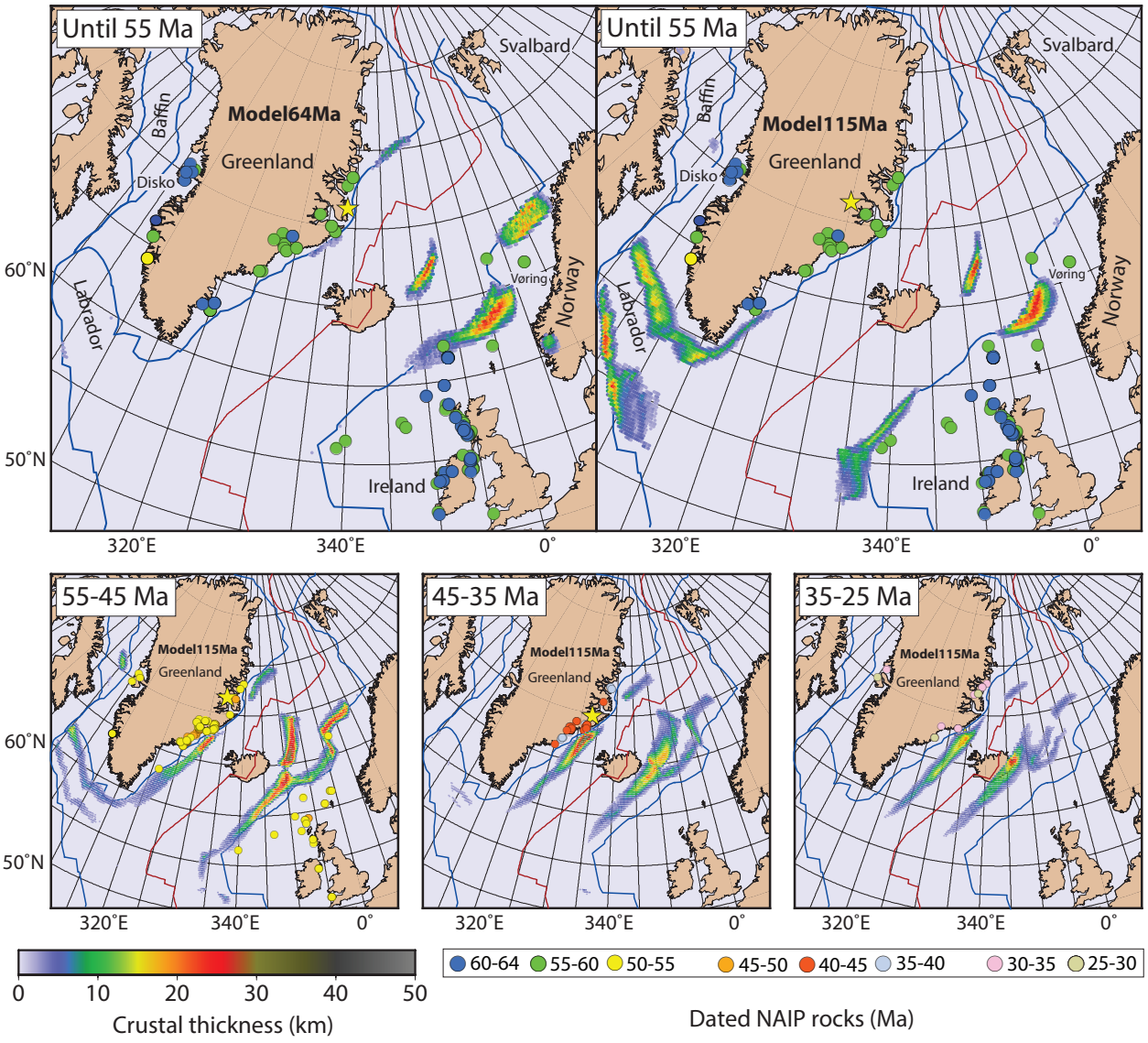
Until 55 Ma
Model64Ma
Greenland
Baffin
Disko
Svalbard
Labrador
Ireland
Norway
Vøring
60˚N
50˚N
320˚E
340˚E
0˚
Until 55 Ma
Model115Ma
Greenland
Baffin
Disko
Svalbard
Labrador
Ireland
Norway
Vøring
55-45 Ma
Model115Ma
Greenland
45-35 Ma
Model115Ma
Greenland
35-25 Ma
Model115Ma
Greenland
0
10
20
30
40
50
Crustal thickness (km)
60-64
55-60
50-55
45-50
40-45
35-40
30-35
25-30
Dated NAIP rocks (Ma)

Figure 6

# Supplementary information to

# Widespread volcanism in the Greenland-North Atlantic region explained by the Iceland plume

Bernhard Steinberger[1,2,*], Eva Bredow[1,3], Sergei Lebedev[4], Andrew Schaeffer[5] & Trond H. Torsvik[2,1,6,7]

[1]*Section 2.5 Geodynamic Modelling, GFZ German Research Centre for Geosciences, Potsdam, Germany.*

[2]*Centre for Earth Evolution and Dynamics (CEED), University of Oslo, Oslo, Norway.*

[3]*Current Address: Institute of Geosciences, Christian-Albrechts-Universitt Kiel, Germany.*

[4]*Dublin Institute for Advanced Studies, School of Cosmic Physics, Geophysics Section, Dublin, Ireland.*

[5]*Department of Earth Science, University of Ottawa, Ottawa, Canada.*

[6]*Geological Survey of Norway (NGU), Trondheim, Norway*

[7]*School of Geosciences, University of Witwatersrand, Wits, South Africa*

**Supplementary movie:** Top view of numerical model development showing the extent of the plume, melt fraction, lithosphere thickness, plate velocities and plate boundaries through time. Further details as in Figure 4.

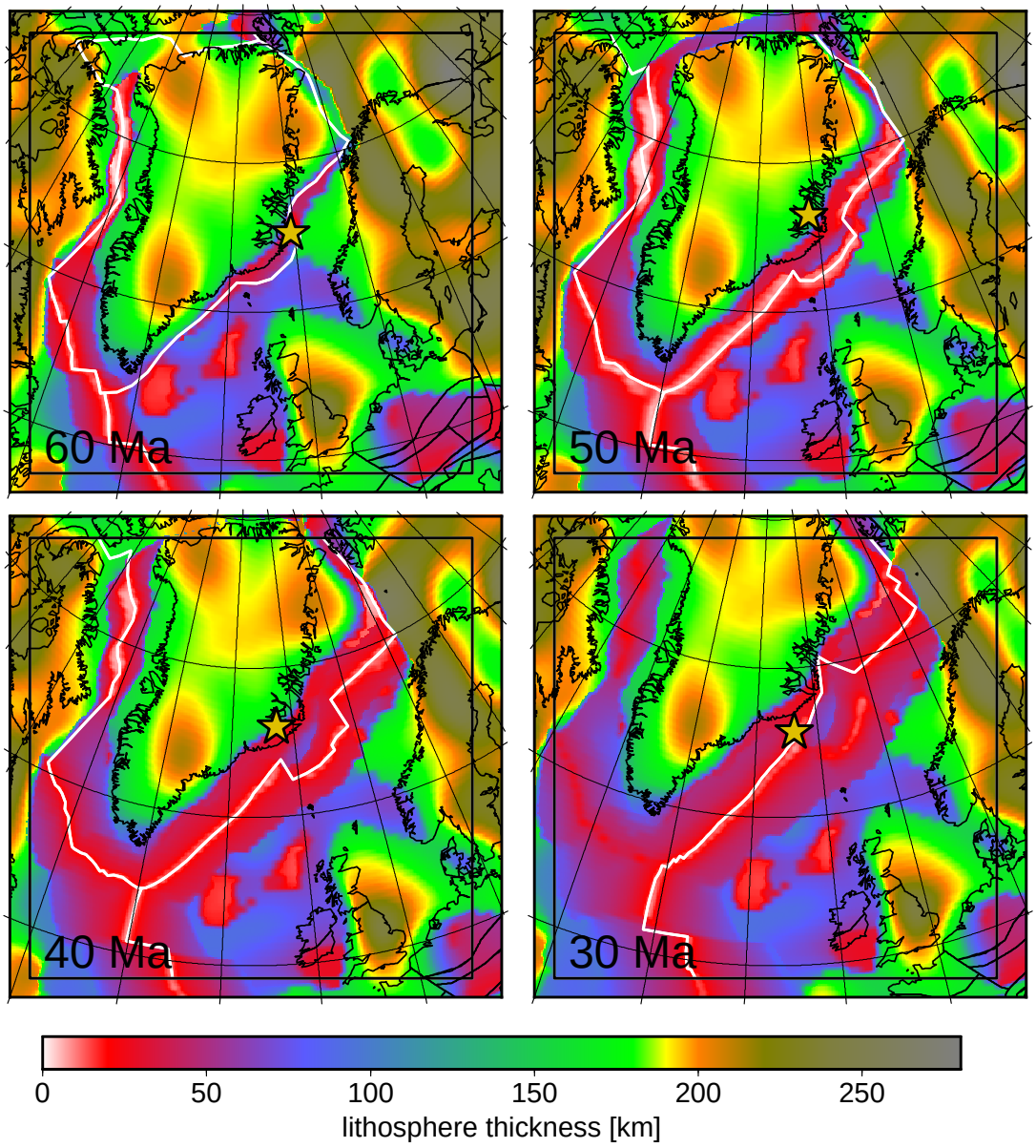


Figure S 1: Lithosphere thickness, ridge location and plume position as in Figure 2 (left), but also shown for 50 Ma, 40 Ma and 30 Ma.

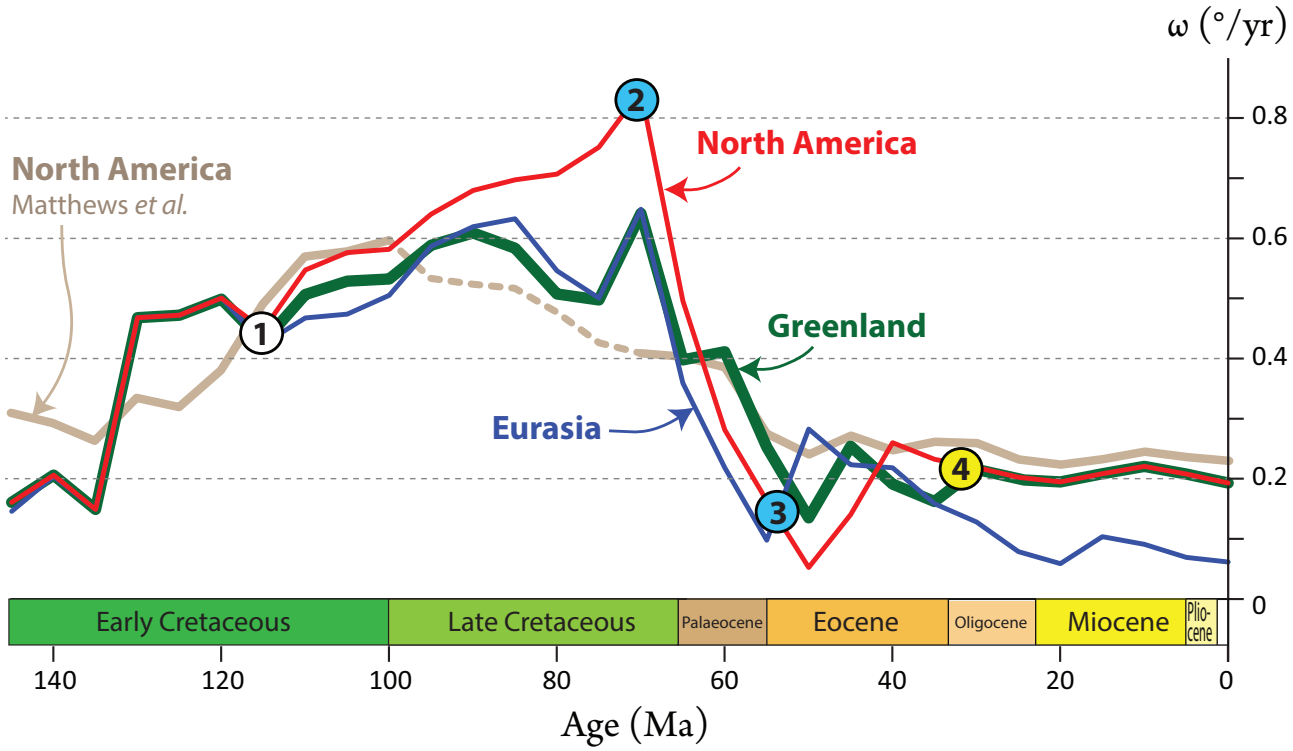
ω (°/yr)
0.8
0.6
0.4
0.2
0
North America
Matthews et al.
North America
Greenland
Eurasia
1
2
3
4
Early Cretaceous
Late Cretaceous
Palaeocene
Eocene
Oligocene
Miocene
Plio-cene
140
120
100
80
60
40
20
0
Age (Ma)

Figure S 2: Absolute angular velocities ($\omega$) for North America, Greenland and Eurasia since the Early Cretaceous (145 Ma). Based on a true polar wander corrected palaeomagnetic reference frame[1] before 120 Ma and a global moving hotspot reference frame (GMHRF[2]) thereafter, interpolated to 5 Ma. The latter is based on five hotspot tracks, including the New England Seamount Chain that directly link North America to the GMHRF. Conversely Greenland and Eurasia are linked to the GMHRF by relative plate circuits. The largest uncertainties in the relative fits are in the Cretaceous which include estimates of pre-drift extension between North America-Greenland and Greenland-Eurasia from the Early Cretaceous (white circle marked 1) to the Early Eocene (blue circle marked 3) when seafloor spreading was initiated between Greenland and Eurasia. Seafloor spreading between North America and Greenland (Labrador Sea and Baffin Bay) probably started in Late Cretaceous (blue circle marked 2) or possible Early Palaeocene time, and terminated in the Early Oligocene (white circle marked 4) when Greenland once again became part of the North American plate. In our preferred plate model, the North Atlantic continents show velocity accelerations during the Cetaceous with peak velocities in the Late Cretaceous and pronounced deceleration during the Palaeocene. The Late Cretaceous peak is not seen in the model of Matthews et al.[3] but in this model they used an older GMHRF[4] back to 70 Ma and then linearly interpolated (smoothed) this GMHRF backward to the true polar wander corrected palaeomagnetic reference frame[1] at 100 Ma (stippled grey line in diagram). It is also worth noting that this older GMHRF[4] did not include the New England Seamount Chain and based on four hotspot tracks linked to the Hawaiian and Louisville hotspots (Pacific Ocean) and to the Reunion (Indian) and Tristan (Atlantic) hotspots.

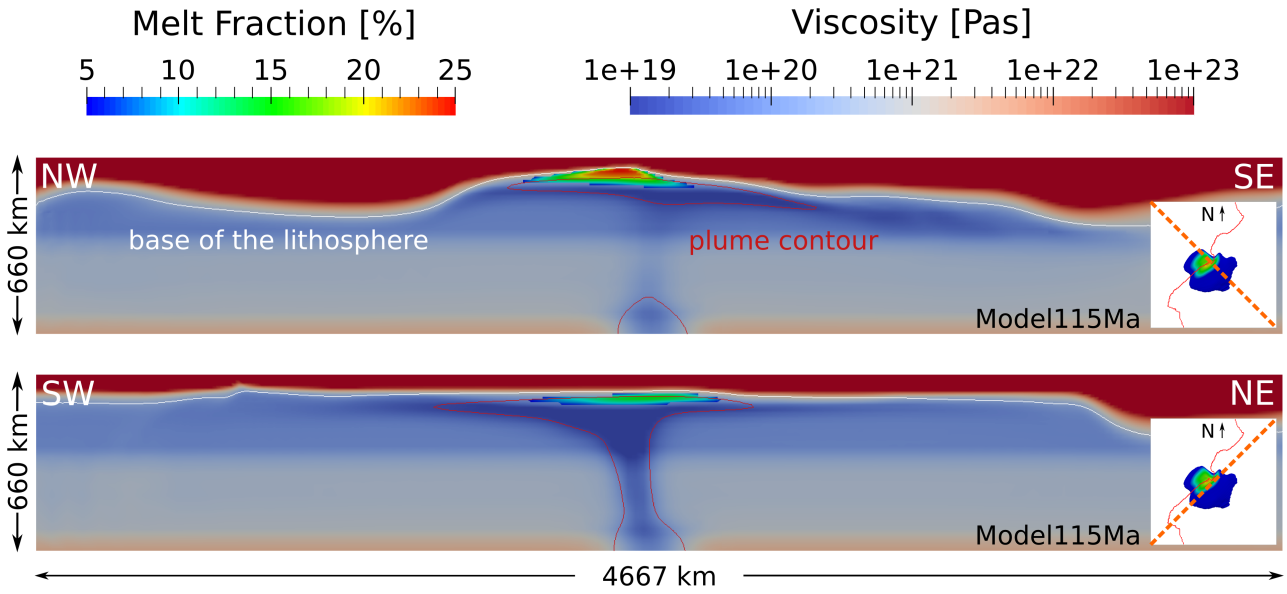


Figure S 3: Cross sections through the modelled Iceland plume (present-day) showing viscosity and melting distribution.

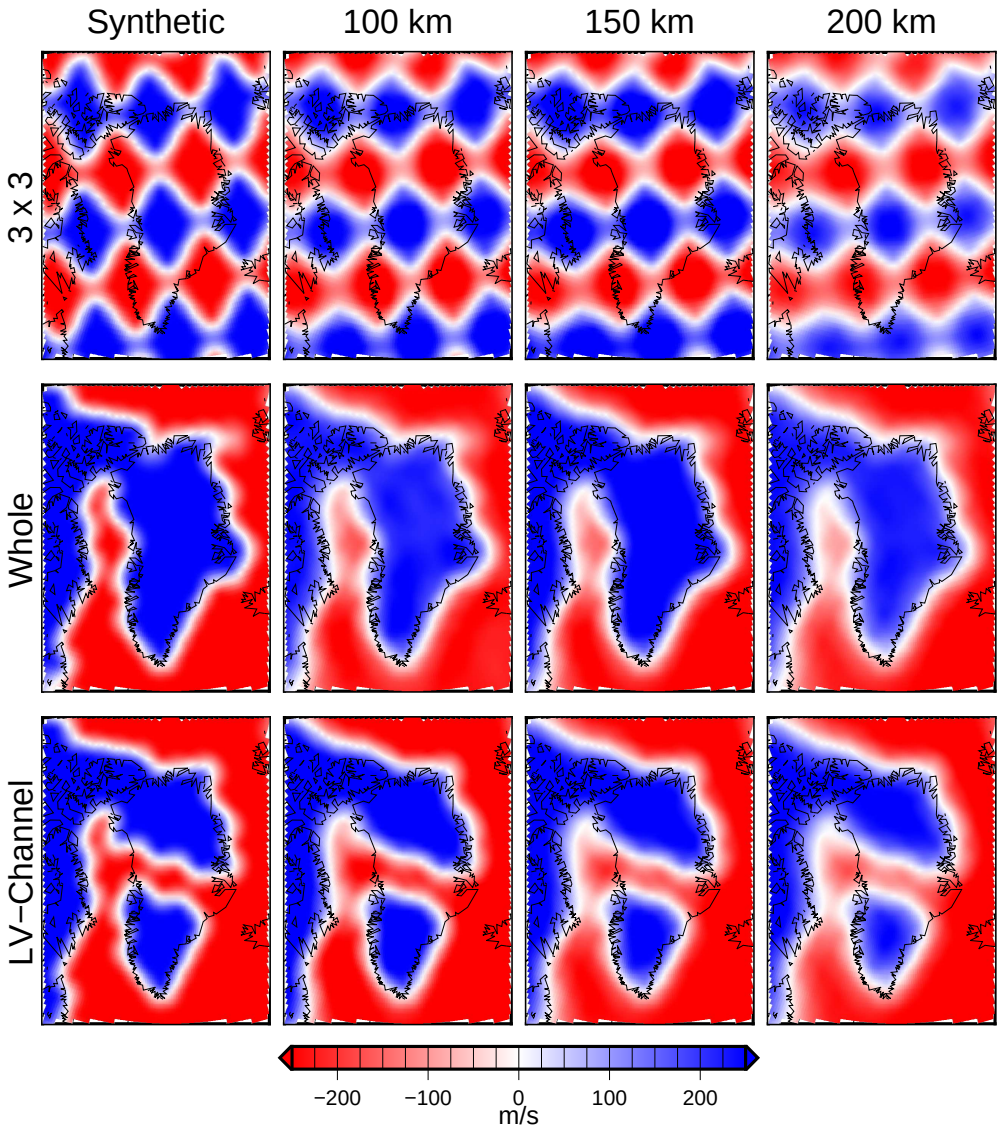
Synthetic
100 km
150 km
200 km
3 x 3
Whole
LV−Channel
−200
−100
0
100
200
m/s

Figure S 4: Results for resolution tests carried out for the AMISvArc Model. The left column shows the three different input models, from top to bottom: a three-by-three knot checkerboard, a structure test for a completely high velocity Greenland, and finally a structure test for Greenland dissected by a low-velocity channel. For each synthetic test, the high velocity anomalies in the synthetic model $\mathbf{m}_S$ are set at 250 m/s and the low velocity anomalies at -250 m/s, across the depth range 80 to 260 km. Using these (noise-free) synthetic starting models (left panels), synthetic data $\mathbf{d}_S$ are computed through multiplication with the kernel matrix $\overline{\overline{\mathbf{A}}}$, as $\mathbf{d}_S = \overline{\overline{\mathbf{A}}}\,\mathbf{m}_S$ (e.g.,[5]). The resulting data, $\mathbf{d}_S$, are inverted using the identical parametrization and regularization as the AMISvArc inversion. The recovered structures at 100, 150, and 200 km depth are illustrated in the righthand three columns. In all cases, there is a slight reduction in overall amplitudes, however, the shape of anomalies remains well recovered. Critically, we note that in the structure tests we clearly differentiate with our dataset the existence of the reduced velocity channel crossing central Greenland from east to west. If no channel is present (row 2), we recover a model which shows no indication for a reduced velocity channel. Furthermore, when imposing a channel in the starting model (row 3), we clearly recover that same channel. In the checkerboard test, the three-by-three checkers are almost perfectly recovered, though amplitudes decrease slightly at greater depths (200 km).

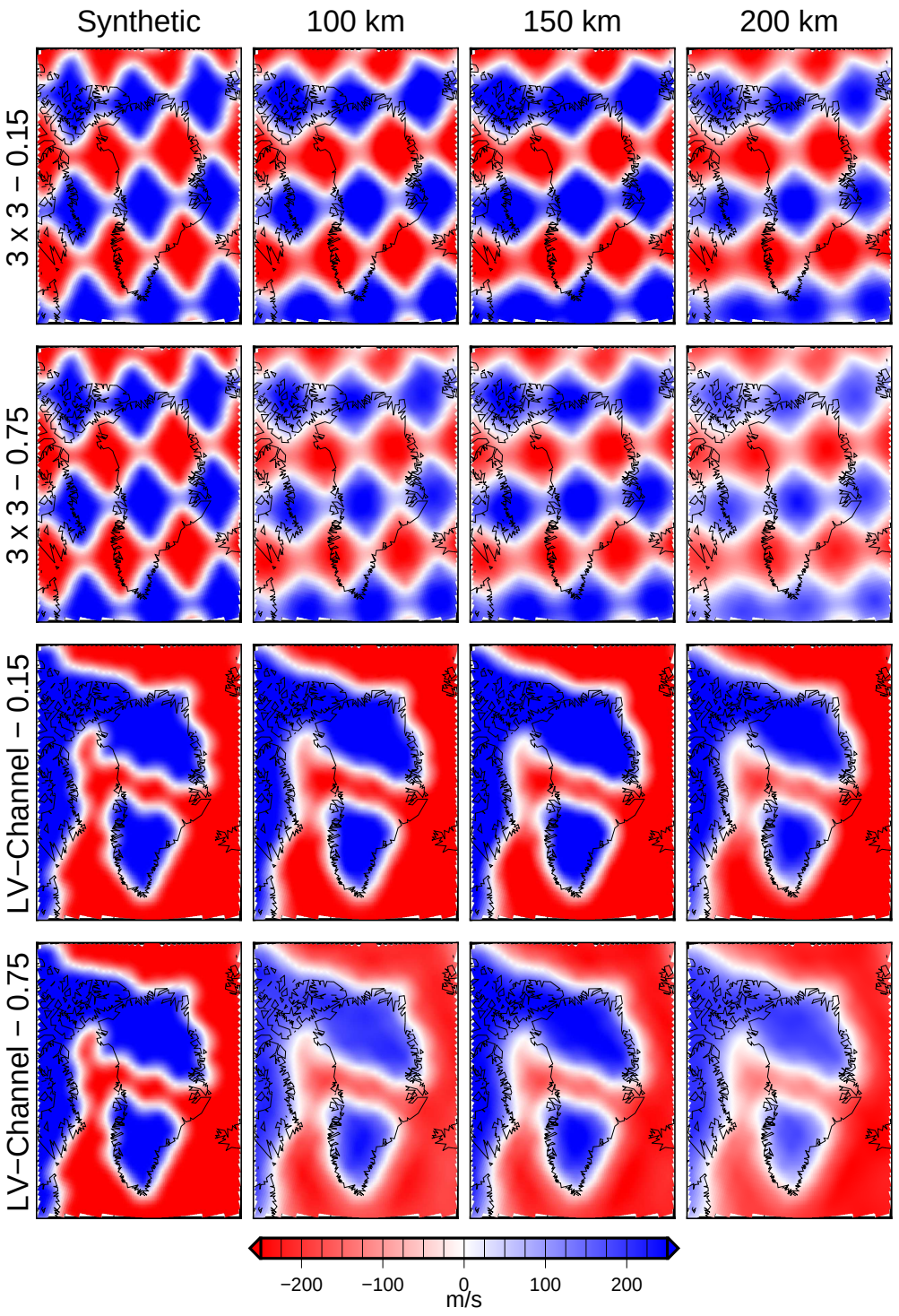
Synthetic
100 km
150 km
200 km
3 x 3 – 0.15
3 x 3 – 0.75
LV–Channel – 0.15
LV–Channel – 0.75
−200
−100
0
100
200
m/s

Figure S 5: Additional resolution tests carried out for the AMISvArc Model with Noise added to the synthetic data. As with Figure 4, the left column shows the input models: two versions of three-by-three checkerboard and two versions of the structural test for Greenland dissected by a low-velocity channel. Each of the synthetic tests were carried out identically to those in Figure 4 above, except that prior to inverting the synthetic data for each model, $\mathbf{m}_S$, random noise was added. The inversion procedure utilized here combines the results of the AMI waveform fitting procedure; as each waveform fit is orthogonalized onto individual basis functions, the resulting synthetic data vector in the inversion is not cast in units of m/s, and therefore difficult to add a specific and quantifiable amount of noise to in m/s (see [5–7] for more information). Therefore, we instead compute the standard deviation of the synthetic data vector $\sigma_S$, then draw a Gaussian distribution of random noise with a standard deviation of 15% and 75% of $\sigma_S$. The synthetic inversions are then carried out on these noisy data, in the same standard manner as for the noise-free case, with the results indicated by the rows "0.15" and "0.75." The results demonstrate that for relatively small amounts of noise (15% $\sigma_S$), the input solution is recovered almost exactly for both the three-by-three checkerboard and the low-velocity channel due in large part to the robust over-sampling of the study region. In the case of the greater amount of noise (75% $\sigma_S$), the shape of the input solution is recovered accurately, although the amplitudes are reduced due to the noise-induced inconsistency of the data.

## Supplementary References


1. Torsvik, T. H. *et al.* Phanerozoic polar wander, paleogeography and dynamics. *Earth Sci. Rev.* **114**, 325–368 (2012).

2. Doubrovine, P. V., Steinberger, B. & Torsvik, T. H. Absolute plate motions in a reference frame defined by moving hot spots in the Pacific, Atlantic, and Indian oceans. *J. Geophys. Res.* **117**, B09101 (2012).

3. Matthews, K. J. *et al.* Global plate boundary evolution and kinematics since the late Paleozoic. *Global Planet. Change* **146**, 226–250 (2016).

4. Torsvik, T. H., Müller, R. D., Van der Voo, R., Steinberger, B. & Gaina, C. Global plate motion frames: Toward a unified model. *Rev. Geophys.* **46**, RG3004 (2008).

5. Schaeffer, A. J. & Lebedev, S. Global shear speed structure of the upper mantle and transition zone. *Geophys. J. Int.* **194**, 417–449 (2013).

6. Lebedev, S., Nolet, G., Meier, T. & van der Hilst, R. D. Automated multimode inversion of surface and S waveforms. *Geophys. J. Int.* **162**, 951–964 (2005).

7. Lebedev, S. & van der Hilst, R. D. Global upper-mantle tomography with the automated multimode inversion of surface and s-wave forms. *Geophys. J. Int.* **173**, 505–518 (2008).